C. R. Chimie 16 (2013) 159–175

Contents lists available at SciVerse ScienceDirect

Comptes Rendus Chimie

www.sciencedirect.com

Full paper/Mémoire

Synthesis, characterization, thermal, electrochemical, and DFT studies of mononuclear cyclopalladated complexes containing bidentate phosphine ligands and their biological evaluation as antioxidant and antibacterial agents

Seyyed Javad Sabounchei [a,*], Mohsen Ahmadi [a], Zahra Nasri [b], Esmaeil Shams [b], Sadegh Salehzadeh [a], Yasin Gholiee [a], Roya Karamian [c], Mostafa Asadbegy [c], Sepideh Samiee [d]

[a] Faculty of Chemistry, Bu-Ali Sina University, Hamedan 65174, Iran
[b] Chemistry Department, University of Isfahan, Isfahan 81746-73441, Iran
[c] Department of Biology, Faculty of Science, Bu-Ali Sina University, Hamedan 65174, Iran
[d] Department of Chemistry, Faculty of Science, Shahid Chamran University, Ahvaz, Iran

ARTICLE INFO

Article history:
Received 15 August 2012
Accepted after revision 15 October 2012
Available online 13 December 2012

Keywords:
DPPH free radical scavenging
Bacterial resistance
Crystal structure
GIAO NMR studies
Interaction energy
Distorted square planar complexes

ABSTRACT

The non-symmetric phosphorus ylides and their Pd(II) complexes have been synthesized as potential antioxidant and antibacterial compounds and their structures were elucidated using a variety of physicochemical techniques. The reaction of 1 equiv non-symmetric phosphorus ylides, $Ph_2PCH_2PPh_2C(H)C(O)PhX$ (X = Br (**Y**^{1}), Cl (**Y**^{2}), NO_2 (**Y**^{3}), OCH_3 (**Y**^{4})) with $[Pd(dppe)Cl_2]$ (**M**^{1}), followed by treatment with 2 equiv AgOTf led to monomeric chelate complexes, $[(dppe)Pd(Ph_2PCH_2PPh_2C(H)C(O)PhX)](OSO_2CF_3)_2$ (X = Br (**C**^{1}), Cl (**C**^{2}), NO_2 (**C**^{3}), OCH_3 (**C**^{4})), which contain a five-membered P,P chelate ring in one side and a five-membered P,C chelate ring in the other side. Palladium ion complexes were synthesized and investigated by cyclic voltammetry, FT-IR, UV–visible, multinuclear (^{1}H, ^{31}P and ^{19}F) NMR, thermal analysis and ESI-mass spectroscopic studies. Some complexes and ligands have been studied by powder XRD and single crystal X-ray diffraction techniques. FT-IR and ^{31}P NMR studies revealed that the ylides **Y** are coordinated to the metal ions via the terminal phosphorus (P_c) of the ylides and methene group (CH). The proposed coordination geometry around the Pd atom in these complexes is defined as slightly distorted square planar by UV-Visible and DFT studies. Thermal stability of all complexes was also shown by TG/DTG methods. Furthermore, the electrochemical behavior of the complexes was investigated by cyclic voltammetry. The results indicate that all complexes are successfully synthesized from the initial ligands. All complexes were analyzed for their antioxidant properties by DPPH free radical scavenging assay. In addition, the antibacterial effects of the hexane-solved complexes were investigated by disc diffusion method against four Gram positive and negative bacteria. All complexes represented antibacterial activity against bacteria tested especially on Gram positive ones. A theoretical study on the structure, ^{1}H and ^{31}P NMR chemical shifts and the interaction energy between the Pd^{2+} ion and ligands dppe and ylide **Y** is also reported.

* Corresponding author.
E-mail address: jsabounchei@yahoo.co.uk (S.J. Sabounchei).

1631-0748/$ – see front matter
http://dx.doi.org/10.1016/j.crci.2012.10.006

1. Abbreviations

DFT	Density Functional Theory
DPPH	1,1-diphenyl-2-picrylhydrazyl
TBATFB	tetrabutylammonium tetrafluoroborate
OTf = OSO_2CF_3	trifluoromethanesulfonate
dppe	1,1-Bis(diphenylphosphino)ethane
MLCT	Metal Ligand Charge Transfer
LMCT	Ligand Metal Charge Transfer
GIAO	Gauge Independent Atomic Orbital
TMS	Tetrametylsilane
SVP	Split-Valence plus Polarization
TZVP	Triple-Zeta Valence plus Polarization

2. Introduction

The use of cyclopalladated complexes as potential chemotherapeutics is an active area of research. These types of compounds are noted for their pharmacological properties, particularly as antibacterial [1–7], antifungal [3,5], and antitumoral agents [1–5,7,8]. Free radicals and chemical species with one or more unpaired electrons are produced in normal or pathological cell metabolism in different circumstances. Environmental stresses cause the faster generation of free radicals than their degradation in the cell [9]. Free radicals play a crucial role in the development of tissue damage in various human diseases such as cancer, aging, neurodegenerative disease, malaria and arteriosclerosis, and pathological events in living organisms [10]. Antioxidants may have an important role in the prevention of these diseases. There is an increasing interest in the antioxidant effects of compounds, especially natural moieties [11–13]. Inorganic antibacterial materials have several advantages over traditionally used organic agents; for example, chemical stability, thermal resistance, safety to the use and long lasting action period [14]. Bacterial resistance is a major drawback in chemotherapy of infectious disease [15]. The emergence of bacterial resistance to antibiotics and its dissemination, however, are major health problems, leading to treatment drawbacks for a large number of drugs. Currently there has been increasing interest in the use of inhibitors of antibiotic resistance for combination therapy [15–17]. Antibacterial agents are co-administered with an inhibitor that deactivates the bacteria's resistance mechanism and increases the antibacterial agent's effectiveness.

The coordination and organometallic chemistry of stabilized phosphorus ylides have been investigated extensively and their ambidenticity explained in terms of a delicate balance between electronic and steric factors [18–23]. The non-symmetrical stabilized ylides derived from bisphosphines, viz., $Ph_2P(CH_2)_nPPh_2 = C(H)C(O)R$ (n = 1, 2) (R = Me, Ph or OMe) [24] form an important class of such ligands which can exist in ylidic and enolate forms. These ligands can therefore engage in different types of bonding [25]. The P, C bonding mode (Scheme 1) had been previously observed for Rh(I), Pd(II), Pt(II), Hg(II) [24–35] and also, the dppe chelating mode with Pd(II) has been found before [36]. The remarkable change in reactivity arises from a subtle variation in the molecular electronic structure of the ylide due to the presence of additional keto stabilization.

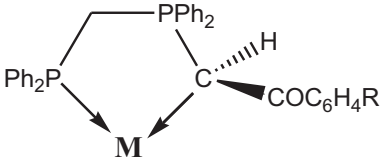

P, C-bonding, Chelate
R = Cl, Br, NO_2, OCH_3

Scheme 1.

As part of this ongoing study we have chosen to investigate the bonding modes adopted by bifunctionalized ylide when coordinate to Pd(II). We have recently investigated the reaction chemistry of palladium(II) chloride complexes containing chelating non-symmetrical phosphorous ligands [25]. In this work, the dppe palladium halide complexes were usually reacted with OTf to extract the AgCl first. Then, the product was used as starting materials to react with non-symmetric phosphorus ylides to form chelated complexes. The results of these studies including the full characterization of the obtained complexes are presented. In addition, antioxidant and antibacterial activities of the synthesized complexes were assessed in vitro.

3. Experimental

3.1. Chemistry

In this study, four Pd(II) complexes with the dppe and the phosphorus ylides derived from the reaction between dppm and α-bromoketo derivatives, [(dppe)Pd($Ph_2PCH_2PPh_2C(H)C(O)PhX$)]$(OTf)_2$ (X = Br (**C^1**), Cl (**C^2**), NO_2 (**C^3**), OCH_3 (**C^4**)), were synthesized and investigated by physicochemical techniques. The reaction between [(dppe)$Pd(OTf)_2$] and ylide (**Y**) in the 1:1 molar ratio readily occurred, leading to the new complexes [(dppe)Pd(Y)]$(OTf)_2$ (Scheme 2).

3.2. Materials and physical measurements

The required chemicals were of analytical reagent grade and were purchased from Merck and Alderich. Melting points were measured on a SMPI apparatus and are reported without correction. Elemental analyses for C, H and N were performed using a Perkin–Elmer 2400 series analyzer. The analyses were repeated twice to check the accuracy of the analyzed data. Fourier transform IR spectra were recorded on a Shimadzu 435-U-04 spectrophotometer and samples were prepared as KBr pellets, in 200–4000 cm^{-1} region. UV-Vis spectra were recorded on a JASCO, V-670 Spectrophotometer, Japan, in the range 190–2700 nm. Mass spectra (electrospray) were recorded from a JEOL JMS 700 B/ES spectrometer. The thermo gravimetric analyses (TGA) were carried out in dynamic nitrogen atmosphere (20 ml min^{-1})

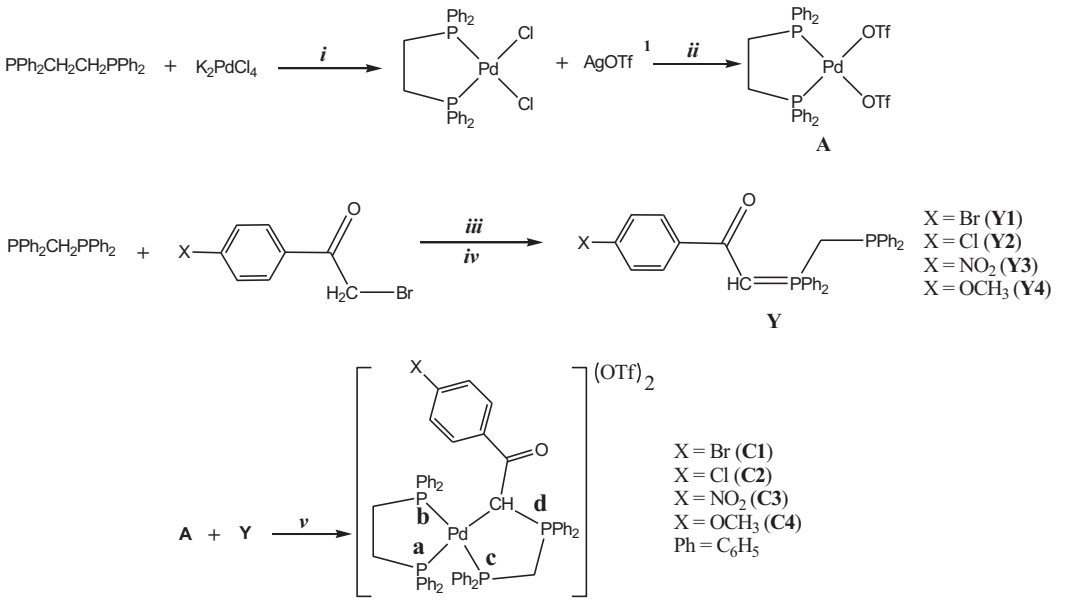

Scheme 2. Synthetic route for preparation of Pd (II) complexes. In order to ease the visualization of the reactions, letter X refer to the substituents on para positions of the phenyl {X = Br (**1**), Cl (**2**), NO_2 (**3**) and OCH_3 (**4**)}. Reagents and conditions: (i) in ethanol, in the presence of hydrochloric acid and using Celite and reflux 8 h; (ii) in dichloromethane, using aluminum foil and Celite, 2 h at 25 °C; (iii) in chloroform, using dry nitrogen atmosphere, 2 h at 25 °C; (iv) in triethyl amine (0.5 ml) in toluene, 15 min in 25 °C; (v) in methanol, using dry nitrogen atmosphere, 12 h at 25 °C. [1] Silver trifluoromethanesulfonate.

with a heating rate of 10 °C min^{-1} in a platinum crucible using Mettler TA-4000/TG-50. The experiments were carried out on samples with an average mass of 10 mg. All electrochemical measurements were performed with a computer-controlled potentiostat, an Autolab electrochemical analyzer model PGSTAT30 (Eco Chemie, Utrecht, The Netherlands) and a standard three electrode cell consisting of an Au working electrode, a platinum wire auxiliary electrode and an Ag/AgCl (3 M KCl) reference electrode. The X-ray powder diffraction pattern was recorded over 2θ = 2–90° range using X-ray diffractometer model APD 2000. Radiation was provided by the copper anode (K_α, λ = 1.54056 Å) operated at 40 kV and 25 MA. NMR Spectra were recorded on a 90 MHz Jeol spectrometer (^{19}F at 84.2 MHz and ^{31}P at 36.26 MHz) or 400 MHz Bruker spectrometer (^1H at 400.13 MHz) in $CDCl_3$ as solvent at 25 °C. The splitting of proton resonances in the ^1H and ^{31}P NMR spectra are shown as: s = singlet, d = doublet, t = triplet and m = multiplet. Chemical shifts (ppm) are relative to internal TMS (δ = 0 (^1H)), $CFCl_3$ (δ = 0 (^{19}F)) and external 85% phosphoric acid (δ = 0 (^{31}P)).

3.3. Crystal structure determination and refinement

Suitable crystals for ligand **Y²** was obtained from dichloromethane solution by slow evaporation of the solvent and mounted in random orientation on glass fibers. The X-ray intensity data were measured at 298 K on a Bruker SMART APEX CCD-based three-circle X-ray diffractometer system using graphite monochromated Mo K_α (λ = 0.71073 Å) radiation. The crystal structures were solved by direct methods and refined by using SHELXS-97 and SHELXL-97 crystallographic software packages [37–40]. All non-hydrogen atoms were refined anisotropically using reflections $I > 2\sigma(I)$. Hydrogen atoms were located in ideal positions.

3.4. Computational details

The geometries of the complex **C²**, phosphorus ylide **Y²** and dppe ligand in the gas phase were fully optimized using SVP and TZVP basis sets [41] at BP86 [42,43] level of theory. All calculations were performed using by Gaussian 03 [44] set of programs. Vibrational frequency analysis, calculated at the same level of theory, indicates that optimized structures are at the stationary points corresponding to local minima without any imaginary frequency. The ^1H and ^{31}P NMR shielding results were obtained at BP86 level of theory and using both the SVP and TZVP basis sets. Both the ^1H and ^{31}P isotropic shielding constants of the optimized mononuclear Pd (II) complex were calculated by using the gauge independent atomic orbital (GIAO) method [45,46].

3.5. Synthesis of phosphorus ylides Y^{1-4}

General procedure [25]: Bis(diphenylphosphino)-methane (dppm) (0.2 g, 0.52 mmol) was dissolved in 5 ml of chloroform and then a solution (5 ml, $CHCl_3$) of 4-bromophenacyl bromide (0.144 g, 0.52 mmol) was added dropwise. The resulting reaction mixture was stirred for 2 h at room temperature. Addition of 25 ml of diethyl ether, after the prescribed reaction time caused the precipitation of the phosphonium salts. The resulting phosphonium salts (0.3 g, 0.45 mmol) were treated with triethyl amine (0.5 ml) in toluene (15 ml). The triethyl amine hydrobromide produced was filtered off and the toluene layer concentrated to 5 ml which upon further addition of petroleum ether (25 ml) resulted in the

precipitation of the ligands as free-flowing solids. The product was collected and dried under vacuum (Scheme 2).

3.6. Synthesis of [Pd(dppe)Cl$_2$] ($\mathbf{M^1}$)

General procedure: to a solution of the Bis(diphenylphosphino)ethane (dppe) (1 g, 2.5 mmol) in 20 ml ethanol was added to a stirred suspension of finely divided K_2PdCl_4 (0.81 g, 2.5 mmol) in 10 ml concentrated hydrochloric acid. The mixture were refluxed with stirring for eight hours and cooled to give precipitates of the product (1.6 g, 90%) (Scheme 2). ^{1}H NMR ($CDCl_3$): δ (ppm) 7.3–7.8 (m, 20H, C_6H_5), 1.82 (m, 4H, CH_2). ^{31}P NMR ($CDCl_3$): δ (ppm) 66.7 (s, PPh_2). Anal. Calc. for $C_{26}H_{24}Cl_2P_2Pd$: C, 54.24; H, 4.20, Found: C, 54.12; H, 4.11%.

3.7. Synthesis of [Pd(dppe)(OTf)$_2$] ($\mathbf{M^2}$)

To a solution of complex $\mathbf{M^1}$ (0.57 g, 1 mmol) in CH_2Cl_2 (20 ml) was added AgOTf (0.51 g, 2 mmol). The reaction mixture was protected from room light with an aluminum foil and stirred for 2 h at room temperature. The solution was then filtered through dry Celite and the solvent was evaporated under reduced pressure. The residue was washed with diethylether (2 × 10 ml) and dried under vacuum (Scheme 2). Product [Pd(dppe)(OTf)$_2$] was obtained as a white powder (0.67 g, 82%). ^{1}H NMR ($CDCl_3$): δ (ppm) 7.3–7.8 (m, 20H, C_6H_5), 1.94 (m, 4H, CH_2). ^{31}P NMR ($CDCl_3$): δ (ppm) 60.1 (s, PPh_2). ^{19}F NMR ($CDCl_3$): δ (ppm) 67.5 (s, CF_3). UV–vis (λmax, nm): 262 (intra-ligand transition, phenyl group), 324 (MLCT). Anal. Calc. for $C_{28}H_{24}F_6O_6P_2PdS_2$: C, 41.88; H, 3.01. Found: C, 41.70; H, 3.11%.

3.8. Synthesis of Pd complexes

3.8.1. Synthesis of [(dppe)Pd(Y^1)](OTf)$_2$ ($\mathbf{C^1}$)

General procedure: to a [Pd(dppe)(OTf)$_2$] (0.4 g, 0.5 mmol) methanol solution (10 ml), a solution of non-symmetric phosphorus ylides ($\mathbf{Y^1}$) (0.29 g, 0.5 mmol) (10 ml, CH_3OH) was added dropwise. The resulting solution was stirred for 12 h at room temperature and then concentrated to a 2 ml in volume and treated with diethylether (2 × 10 ml) to give a final product. The product was collected and dried under vacuum (Scheme 2). White solid (0.58 g, 84%). M.p. 225–227 °C. ^{1}H NMR ($CDCl_3$): δ (ppm) 6.91–7.77 (m, 44H, C_6H_5), 2.66 (m, 2H, CH_2(dppe)), 2.76 (m, 2H, CH_2(dppe)), 4.82 (br, 1H, CH(methine)), 4.63 (m, 2H, CH_2(ylide)). ^{31}P NMR ($CDCl_3$): δ (ppm) 55 (m, P_a), 55.1 (ddd, P_b, $^2J(P_bP_c)$ = 355.1 Hz, $^3J(P_bP_a)$ = 19.73 Hz, $^3J(P_bP_d)$ = 11.96 Hz), 19.15 (ddd, P_c, $^2J(P_cP_b)$ = 354.9 Hz, $^2J(P_cP_a)$ = 58.1 Hz, $^2J(P_cP_d)$ = 27 Hz), 37.65 (ddd, P_d, $^2J(P_dP_b)$ = 58 Hz, $^2J(P_dP_c)$ = 20.14 Hz, $^3J(P_dP_a)$ = 14 Hz). ^{19}F NMR ($CDCl_3$): δ (ppm) -78 (s, CF_3). Selected IR data (KBr, cm^{-1}, w = weak, m = medium, s = strong): ν = 997 (m, P-CH_2), 820 (m, P-CH), 1616 (s, C = O). UV–vis (λmax, nm): 241 (intra-ligand transition, phenyl group), 257 (intra-ligand transition, C = O), 300 (LMCT, s→d), 325 (MLCT). ESI-MS: m/z = 1235.06 ((Calc. 1235), [(dppe)Pd-Y^1]$^+$), 1085.1 ((Calc. 1086), [(dppe)Pd-Y^1]$^{2+}$). Anal. Calc. for $C_{61}H_{51}BrF_6O_7P_4PdS_2$: C, 52.92; H, 3.71. Found: C, 52.81; H, 3.65%.

3.8.2. Data for [(dppe)Pd(Y^2)](OTf)$_2$ ($\mathbf{C^2}$)

White solid (0.53 g, 80%). M.p.: 230–232 °C. ^{1}H NMR ($CDCl_3$): δ (ppm) 6.92–7.78 (m, 44H, C_6H_5), 2.67 (m, 2H, CH_2(dppe)), 2.81(m, 2H, CH_2(dppe)), 4.93 (m, 1H, CH(methine)), 4.52 (m, 2H, CH_2(ylide)). ^{31}P NMR ($CDCl_3$): δ (ppm) 55.2 (m, P_a), 55.0 (ddd, P_b, $^2J(P_bP_c)$ = 357.2 Hz, $^3J(P_bP_a)$ = 20.81 Hz, $^3J(P_bP_d)$ = 13.0 Hz), 19.53 (ddd, P_c, $^2J(P_cP_b)$ = 355.7 Hz, $^2J(P_cP_a)$ = 60.2 Hz, $^2J(P_cP_d)$ = 26.8 Hz), 37.71 [ddd, P_d, $^2J(P_dP_b)$ = 60.5 Hz, $^2J(P_dP_c)$ = 20.5 Hz, $^3J(P_dP_a)$ = 13.9 Hz). ^{19}F NMR ($CDCl_3$): δ (ppm) -77.9 (s, CF_3). Selected IR data (KBr, cm^{-1}): ν = 998 (m, P-CH_2), 821 (m, P-CH), 1616 (s, C = O). UV–vis (λmax, nm): 245 (intra-ligand transition, phenyl group), 260 (intra-ligand transition, C = O), 310 (LMCT, s→d), 330 (MLCT). ESI-MS: m/z = 1191.2 ((Calc. 1191), [(dppe)Pd-Y^1]$^+$), 1041.1 ((Calc. 1040), [(dppe)Pd-Y^1]$^{2+}$). Anal. Calc. for $C_{61}H_{51}ClF_6O_7P_4PdS_2$: C, 54.68; H, 3.84. Found: C, 54.52; H, 3.66%.

3.8.3. Data for [(dppe)Pd(Y^3)](OTf)$_2$ ($\mathbf{C^3}$)

White solid (0.5 g, 75%). M.p.: 240–242 °C. ^{1}H NMR ($CDCl_3$): δ (ppm) 6.95–7.80 (m, 44H, C_6H_5), 2.6 (m, 2H, CH_2(dppe)), 2.8 (m, 2H, CH_2(dppe)), 5.22 (m, 1H, CH(methine)), 4.53 (m, 2H, CH_2(ylide)). ^{31}P NMR ($CDCl_3$): δ (ppm) 60.9 (m, P_a), 59.02 (ddd, P_b, $^2J(P_bP_c)$ = 356.2 Hz, $^3J(P_bP_a)$ = 18.03 Hz, $^3J(P_bP_d)$ = 13.52 Hz), 23.34 (ddd, P_c, $^2J(P_cP_b)$ = 355.3 Hz, $^2J(P_cP_a)$ = 60.4 Hz, $^2J(P_cP_d)$ = 24.76 Hz), 40.94 (ddd, P_d, $^2J(P_dP_b)$ = 60.1 Hz, $^2J(P_dP_c)$ = 18.81 Hz, $^3J(P_dP_a)$ = 13.8 Hz). ^{19}F NMR ($CDCl_3$): δF (ppm) -78 (s, CF_3). Selected IR data (KBr, cm^{-1}): ν = 998 (s, P-CH_2), 827 (m, P-CH)], 1629 (s, C = O)]. UV–vis (λmax, nm): 245 (intra-ligand transition, phenyl group), 255 (intra-ligand transition, C = O), 300 (LMCT, s→d), 340 (MLCT). ESI-MS: m/z = 1202.1 ((Calc. 1200), [(dppe)Pd-Y^1]$^+$), 1050.06 ((Calc. 1051), [(dppe)Pd-Y^1]$^{2+}$). Anal. Calc. for $C_{61}H_{51}F_6NO_9P_4PdS_2$: C, 54.25; H, 3.81. Found: C, 54.69; H, 3.72%.

3.8.4. Data for [(dppe)Pd(Y^4)](OTf)$_2$ ($\mathbf{C^4}$)

White solid (0.57 g, 86%). M.p.: 212–214 °C. ^{1}H NMR ($CDCl_3$): δ (ppm) 6.5–7.82 (m, 44H, C_6H_5), 2.72 (m, 2H, CH_2(dppe)), 2.96 (m, 2H, CH_2(dppe)), 4.71 (m, 1H, CH(methine)), 4.51 (m, 2H, CH_2(ylide)), 3.67 (s, 3H, CH_3). ^{31}P NMR ($CDCl_3$): δ (ppm) 54.6 (m, P_a), 55.16 (ddd, P_b, $^2J(P_bP_c)$ = 359.18 Hz, $^3J(P_bP_a)$ = 22.0 Hz, $^3J(P_bP_d)$ = 11.82 Hz), 19.31 (ddd, P_c, $^2J(P_cP_b)$ = 359.15 Hz, $^2J(P_cP_a)$ = 66.0 Hz, $^2J(P_cP_d)$ = 21.28 Hz), 37.67 (ddd, P_d, $^2J(P_dP_b)$ = 65.3 Hz, $^2J(P_dP_c)$ = 20.2 Hz, $^3J(P_dP_a)$ = 12.9 Hz). ^{19}F NMR ($CDCl_3$): δF (ppm) -78.3 (s, CF_3). Selected IR data (KBr, cm^{-1}): ν = 997 (m, P-CH_2), 825 (s, P-CH), 1594 (s, C = O). UV–vis (λmax, nm): 240 (intra-ligand transition, phenyl group), 265 (intra-ligand transition, C = O), 310 (LMCT, s→d), 350 (MLCT). ESI-MS: m/z = 1035.2 ((Calc. 1036), [(dppe)Pd-Y^1]$^+$), 1185.2 ((Calc. 1185), [(dppe)Pd-Y^1]$^{2+}$). Anal. Calc. for: C, 55.76; H, 4.08. Found: C, 55.62; H, 4.06%.

3.9. Biological studies

3.9.1. DPPH radical scavenging assay

In order to determine the radical scavenging ability, the method reported by Mensor et al. [47] was used. Briefly, 0.3 mM alcohol solution of DPPH (1 ml) was added to samples (2.5 ml) containing different synthesized

Table 1
Comparison $^{31}P\{1H\}$ NMR and IR bands of the phosphorus ylides and chelated complexes.

Complexes & Ligands	$^{31}P\{^1H\}$ NMR, ppm				J (PP), Hz						FT-IR (cm^{-1})	
	δP_a	δP_b	δP_c	δP_d	J_{ab}	J_{ac}	J_{ad}	J_{cd}	J_{bd}	J_{cb}	ν (CO)	ν (PCH)
Y^1			−30.0	11.4				63.7			1502	881
C^1	55.0	55.1	19.1	37.6	19.7	58.1	14.0	27.0	11.9	355.1	1616	820
Y^2			−29.9	11.3				63.1			1503	846
C^2	55.2	55.0	19.5	37.7	20.8	60.2	13.9	26.8	13.0	355.7	1616	821
Y^3			−30.4	11.5				62.5			1524	862
C^3	60.9	58.8	23.8	41.0	18.0	60.4	13.8	24.7	13.5	355.3	1629	827
Y^4			−29.6	11.1				62.4			1507	876
C^4	55.0	55.4	19.3	37.8	22.0	66.0	12.9	21.3	11.8	359.2	1594	825

compounds. The samples were first kept in a dark place at room temperature and their absorbance was recorded at 517 nm after 30 min. The antiradical activity (AA) was determined using the following formula:

$$AA\% = 1 - ((A_s - A_b)/A_c) \times 100$$

Blank samples contained 1 ml methanol + 2.5 ml from various concentrations of synthesized compounds; control sample containing 1 ml of 0.3 mM DPPH + 2.5 ml methanol. The optic density of the samples, the control and the empty samples were measured in comparison with methanol. A synthetic antioxidant, Ascorbic acid was used as positive controls. Experiments were carried out triplicate.

3.9.2. Antibacterial activity

The potential antibacterial effects of the complexes were investigated by disc diffusion method against two strains of Gram-positive bacteria, namely *Bacillus cereus* (PTCC 1247), *Staphylococcus aureus* (Wild) and two strains of Gram negative bacteria, namely *Proteus vulgaris* (PTCC 1079), and *Serratia marcescens* (PTCC 1111) [48]. The complexes were dissolved in hexane to a final concentration of 1 mg/ml and then sterilized by filtration using 0.45 μm Millipore. All tests were carried using 10 ml of suspension containing 1.5×10^8 bacteria per millilitre and spread on nutrient agar medium (NA). Negative controls were prepared by using hexane. Gentamycin and Penicillin were used as positive reference standards.

3.9.3. Statistical analysis

All data, for both antibacterial and antioxidant activity tests, are the average of triplicate analyses. Analysis of variance was performed by Excel and SPSS procedures. The statistical analyses were performed using Student's *t*-test, and P value < 0.05 was regarded as significant.

4. Results and discussion

4.1. FT-IR and ^{19}F NMR studies

The proclivity of the OTf ligand to be replaced by nucleophiles is further shown by some observations indicating that in **M²** the poorly coordinated OTf is continuously being changed with the phosphorus ylides. Fluorine NMR (measured in $CDCl_3$) shows a weak peak for the trifluoromethanesulfonate ion in near 67.5 ppm in case of the complex **M²** (Supplementary material, Fig. S1). ^{19}F NMR spectroscopy in room temperature reveals a single resonance due to OTf at −77.9 ppm in complex **C²** (Fig. S2), which indicates that the trifluoromethanesulfonate is a counter ion [49–51].

The IR spectrum of the ligands (**Y¹-Y⁴**) and their complexes showed a band at ~1500 cm^{-1} assigned to the carbonyl group. The characteristic band at 850 – 900 cm^{-1} of the P–CH group of the phosphorus ylide and its complexes are assigned to P–C vibration (Table 1). The ν (CO), which is sensitive to complexation, occurs around 1600 cm^{-1} in the parent ylides [52,53]. Coordination of the ylide through carbon causes an increase in the ν (CO), while, when O-coordination occurs, a lowering in the value of the ν (CO) would be expected [54]. Thus the IR absorption bands for the complexes at higher frequencies indicate that C-coordination has occurred [33].

4.2. ^{31}P NMR studies

In the $^{31}P\{^1H\}$ NMR spectra of the $Ph_2\mathbf{P}CH_2\mathbf{P}Ph_2C(H)C(O)PhX$ (**Y¹–Y⁴**) the signal due to PCH (P_d) and PCH_2 (P_c) appears as a two doublet in ~ 11 and -30 ppm, respectively (Fig. S3). Also, the ^{31}P chemical shift of **M¹** due to P_a and P_b appears as singlet in 66 ppm (Fig. S4). The ^{31}P NMR spectrum shows an interesting pattern of signals which allows assigning definitely the structure of these complexes (**C¹-C⁴**). The four P atoms in these complexes are chemically and magnetically non-equivalent (Scheme 2); therefore, the ^{31}P $\{^1H\}$ NMR spectrum exhibits four batch-peak (Fig. 1). The upfield peak ($\delta P \approx 55$–60, m), ($\Delta\delta \approx -10$ ppm) is assigned to the P atom (P_a) of the bidentate ligand (dppe), which is directly attached to the Pd centre in the front of CH group and thus shielded. The $^3JP_bP_a$ coupling constant of ~20 Hz lies within the typical values of similar systems [55–57]. Following, the $^2JP_cP_a$ and $^3JP_dP_a$ coupling constant are ~60 and ~13 Hz, respectively [34]. The upfield peak ($\delta P \approx 55$–59, ddd), ($\Delta\delta \approx -8$ ppm) is assigned to the P atom (P_b) of the dppe, which is directly attached to the Pd centre in the front of PCH_2 group (P_c) and thus shielded (Table 1). The extremely strong coupling with the P atom (P_b) of the dppe ligand ($^2JP_bP_c \approx 355$ Hz) can only be rationalized in the

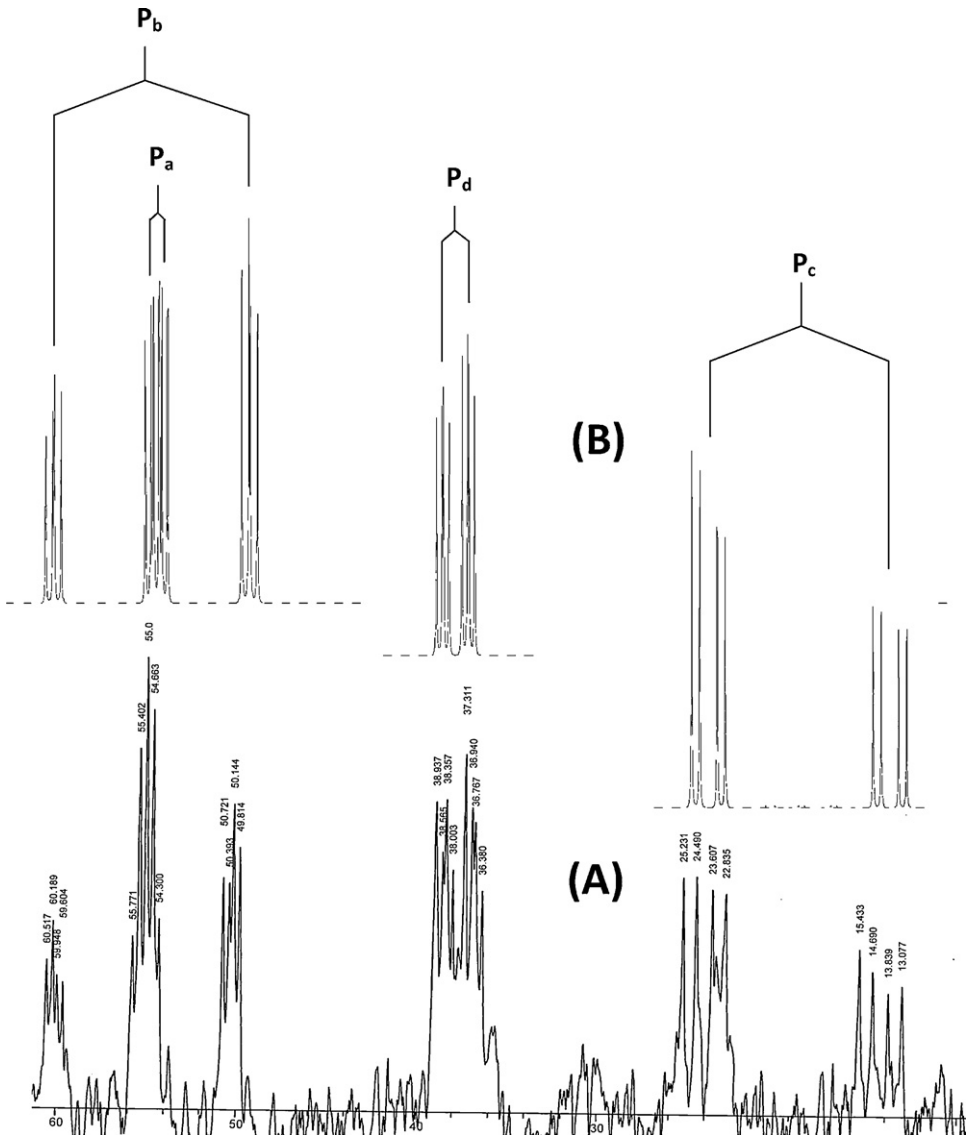

Fig. 1. The $^{31}P\{^{1}H\}$ NMR spectrum of complex **C**[1]. (A): real spectrum; (B): simulated spectrum.

context of a trans arrangement between P_b and P_c [56–64]. The $^{3}JP_bP_d$ coupling constant is ~12 Hz. Two downfield peaks are assigned to two P atoms of the chelate phosphorus ylide. The ylidic P atom (P_d) of the phosphorus ylide is not directly coordinated to the metal centre, thus coupling with Pc is weak ($^{2}JP_dP_c \approx 24$ Hz) as expected [34]. Coupling with P_b ($^{3}JP_dP_b \approx 12$) and Pa ($^{3}JP_dP_a \approx 13$ Hz) gives rise to a downfield ddd-peak ($\delta P \approx 37$–41, ddd), ($\Delta\delta \approx +30$ ppm). The chemical shifts for the two non-equivalent P-atoms of the ambidentate P,CH-ligand are assigned on the basis of published NMR data for these complexes [25]. Finally, the downfield peak ($\delta P \approx 19$–24, ddd), ($\Delta\delta \approx +50$ ppm) is assigned to PCH (P_c).

The significant downfield shift of the signal from that of the free ylide is in agreement with the C-bonding of the ylides. The coordination via the phosphine moiety is also clearly evidenced from the strong downfield shifts of the signal due to PPh_2 group when compared to that of the same signal in the free ylide [33,58].

4.3. ^{1}H NMR studies

The d^8 distorted square planar palladium(II) complexes are all diamagnetic and give resolved NMR spectra which confirm the nature of the binding [65]. Regarding the ^{1}H NMR spectrum of these complexes, the phenyl protons of the dppe ligand and phosphorus ylide are observed in the aromatic region of the spectrum, between 6.5–8.0 ppm [25]. According to the published data, the ^{1}HNMR spectrum of the palladium(II) complexes was consistent with coordination of the phosphorus ylide to the metal through the CH and P_c atoms. In the ^{1}H NMR spectrum, the signal due to the methene proton for complex **C**[1] is broad

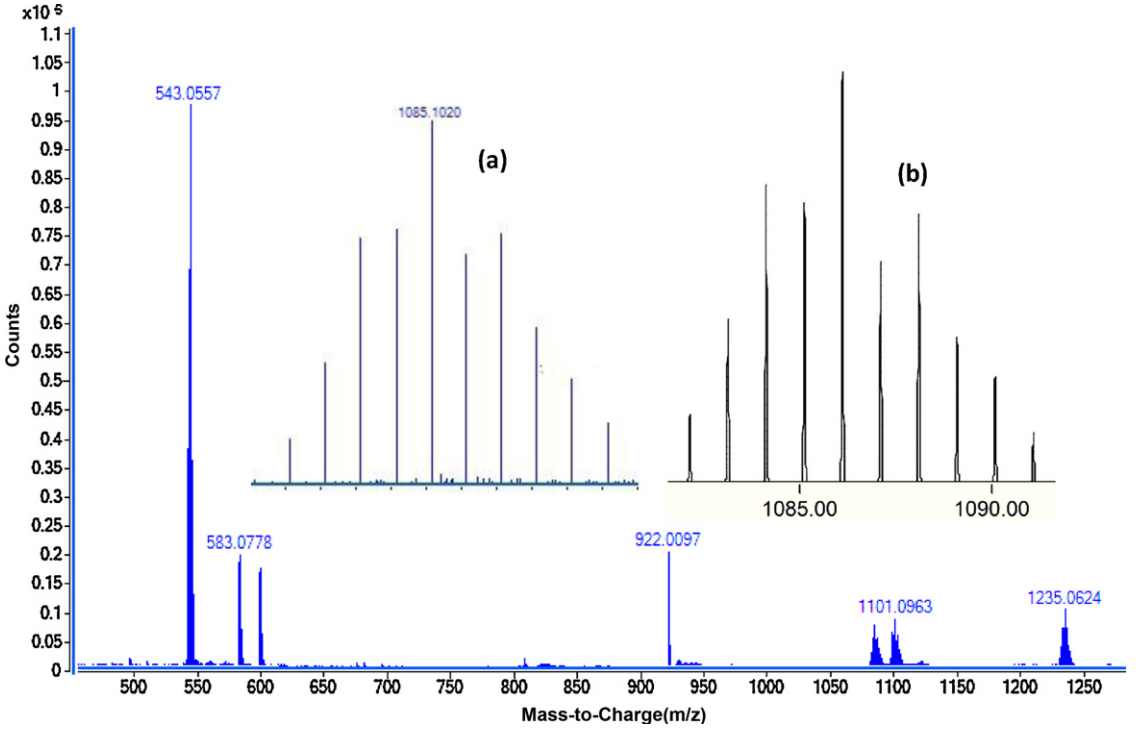

Fig. 2. ESI-MS (dilute THF) of complex $\mathbf{C^1}$. The inset spectrum shows the overlaid experimental (**a**) and calculated (**b**) isotope patterns for $[Pd(dppe)(\mathbf{Y^1})]^{2+}$.

[25]. Similar behavior was observed earlier in the case of ylide complexes derived from $PtCl_2$ [66], whereas the complexes $\mathbf{C^2}$-$\mathbf{C^4}$ showed a multiple peak in ~4.9 ppm due to the methene proton. The expected lower shielding of the ^1H nuclei for the PC(H) group upon complexation in the case of C-coordination was observed in their corresponding spectra [67]. All complexes showed a multiple peak in near 2–4 ppm due to CH_2 groups of the dppe ligand (e.g. complex $\mathbf{C^4}$, Fig. S5). The CH_2 protons in all complexes of the phosphorus ylide appear as a multiplet (m) $\delta \approx 4.5$ ppm (Fig. S5). A singlet appeared at 3.67 ppm corresponding to methyl group of protons in complex $\mathbf{C^4}$.

4.4. ESI mass spectrometry

The positive ion electrospray-mass spectra (ESI^+-MS) of the complexes $\mathbf{C^1}$–$\mathbf{C^4}$ were recorded as very dilute THF solution. The molecular ion was observed in the ESI mass spectra of all complexes. The phosphorus ylide $\mathbf{Y^1}$ has a molecular ion peak at *m/z* 583. The mass spectrum of complex $\mathbf{C^1}$ was characterized by the appearance of the fragment at *m/z* 1085.1 owing to the removal of two OTf group and $[(dppe)Pd\text{-}Y^1]^{2+}$ was formed. A peak at *m/z* 1235.06 related to the molecular ion corresponds to elimination of one OTf ions to give $[(dppe)Pd\text{-}Y^1]^+OTf$. Similar fragmentation patterns are observed for complexes $\mathbf{C^1}$–$\mathbf{C^4}$ and closely matched to what is expected and clearly confirmed the formation of these compounds. Modeling pattern of the complex $\mathbf{C^1}$ and $\mathbf{C^4}$ are presented in Fig. 2 and Fig. S6, respectively.

4.5. Electronic absorption

All palladium complexes have been found to be diamagnetic indicating a +2 oxidation state for palladium. The electronic spectra of the complexes have been recorded in solid state and displayed three bands in the region around 200–500 nm. The electronic spectra of the phosphorus ylides as a ligand showed spectral bands due to $\pi \rightarrow \pi^*$ and $n \rightarrow \pi^*$ transitions (Fig. S7). On complexation these bands are shifted (Fig. S7). The strong charge transfer transitions may interfere and prevent the observation of all the expected bands [68–70]. The strong bands ~400 nm is assignable to a combination of metal ligand charge transfer (MLCT) and d-d [68,71]. The broad band at 330–370 nm (28,700 cm^{-1}) is assignable to combination of phosphor/metal charge transfer (L_πMCT) and d-d bands. The broad band that appeared around 470 nm (21,250 cm^{-1}) has been reported as due to both distorted square planar and undistorted square planar Pd(II) complexes [72,73]. The bands that appeared around 250, 350 and 450 nm have been assigned to intra-ligand transition, [74,75] LMCT [74–76] and MLCT [77,78], respectively. The two bands between 230 and 260 nm (39,000–42,200 cm^{-1}) in the Pd(II) complexes are assigned to ligand centered transitions (π-π^* and n-π^*).

The band near 31,740 cm^{-1} in complex $\mathbf{C^1}$ is spin-allowed transition; $a_{1g}(d_{x^2-y^2}) - b_{1g}(d_{x^2-y^2})$ i.e. $^1A_{1g} \rightarrow {}^1B_{1g}$. The broad bands between 340 and 360 nm (27,700–29,400 cm^{-1}) in the palladium complexes are assignable to a combination of MLCT and $e_g(d_{yz},d_{xz}) - b_{1g}(d_{x^2-y^2})$, i.e. $^1A_{1g} \rightarrow {}^1E_g$ bands. Therefore, the electronic spectra of Pd (II)

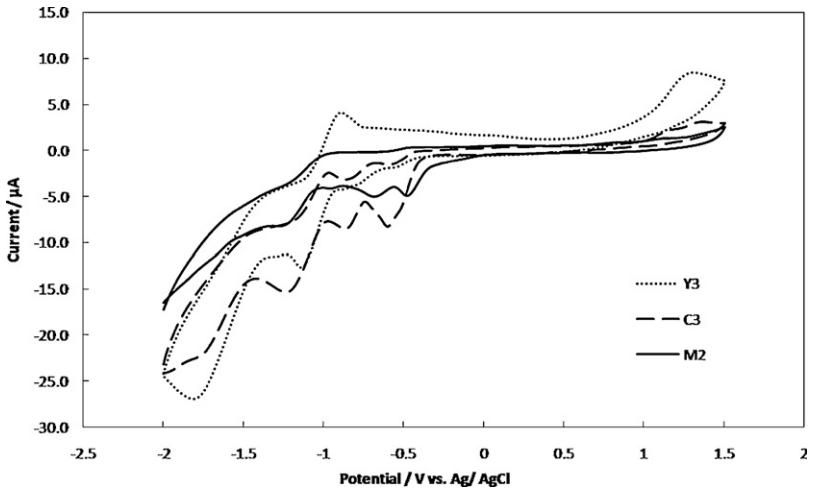

Fig. 3. Cyclic voltammograms of 1 mM of $\mathbf{M^2}$, $\mathbf{Y^3}$ and $\mathbf{C^3}$ in dichloromethane containing 0.1 M TBATFB as supporting electrolyte, at the Au electrode and scan rate of 100 mV/s.

complexes are indicative of distorted square planar geometry [79–81].

4.6. Electrochemical studies

Electrochemical studies of $\mathbf{M^2}$, phosphorus ylides as ligand ($\mathbf{Y^1}$-$\mathbf{Y^4}$) and Pd (II) complexes ($\mathbf{C^1}$-$\mathbf{C^4}$) have been carried out by cyclic voltammetry (CV) in dichloromethane solution, containing 0.1 M tetrabutylammonium tetrafluoroborate (TBATFB) as supporting electrolyte using Au working electrode and Pt wire counter electrode. All the potentials were referenced to Ag/AgCl reference electrode.

Cyclic voltammograms of 1 mM of $\mathbf{M^2}$, $\mathbf{Y^3}$ and $\mathbf{C^3}$ in dichloromethane, containing 0.1 M TBATFB at a scan rate of 100 mV/s is shown in Fig. 3. For the complex $\mathbf{M^2}$ the cathodic potential peak corresponds to the redox pair of Pd(II)/Pd(I) appeared at −0.65 V vs. Ag/AgCl. That reduction was due to one electron transfer process. When the potential was scanned further in the cathodic direction, a second cathodic potential peak at −1.12 V was observed, which corresponds to the redox pair of Pd(I)/Pd(0). There were no anodic peaks observed on the reverse scan [82]. This behavior is similar to that reported previously in cyclic voltammetric study of various types of Pd(II) complexes in aprotic solvents [82–84]. This irreversibility may be due to the reaction of a Pd(0) complex with adventitious O_2 or other components of the solution. Another cathodic peak observed at −0.45 V is corresponding to the reduction of dppe ligand.

For $\mathbf{Y^3}$, the cyclic voltammogram displayed two irreversible and quasi reversible reduction peaks at −1.65 V and −1.10 V, respectively. The first peak could be assigned to a four-electron reduction of nitro group generating the hydroxylamine derivative according to:

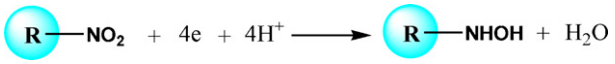

The second cathodic peak assigned to the further reduction of the hydroxylamine to p-amino derivative [7,85].

In addition, the CV of the $\mathbf{C^3}$ exhibited an irreversible reduction peak at −1.60 V corresponding to the reduction of nitro group. The reduction process is shifted towards lower potential revealed an enhancement of the reduction process in the presence of palladium [7]. The disappearance of the second reduction peak of nitro group indicated the participation of the hydroxylamine group in the complex formation.

The quasi reversible reduction peaks at −0.82 V and −1.18 V can be assigned to the formation of Pd(I) from Pd(II) and formation of Pd(0) from Pd(I), respectively. The irreversible cathodic peak at −0.55 V is corresponding to the reduction of dppe ligand. The reduction process is shifted toward more negative potential in the presence of nitro group. The existence of the cathodic peaks of Pd, NO_2 and the dppe in the CV of the $\mathbf{C^3}$ complex, is an evidence for the synthesis of this complex. The cyclic voltammetric data of metal center for the other complexes are given in Table 2.

4.7. Thermal analyses

Thermal stability of the complexes was determined by TG/DTG studies from 25–1000 °C. The compounds were heated to 950–1000 °C, all relevant weight loss was completed by 800 °C. Discussing the simultaneous TG/DTG curves constructed for phosphorus ylide ($\mathbf{Y^1}$), one can observe two endothermic mass loss stages (supplementary material, Fig. S8). The 1st decomposition step at 80–710 °C

Table 2
Electrochemical data of the palladium (II) complexes.

Complex	E_{pc} Pd^{II}-Pd^{I} (V)	E_{pc} Pd^{I}-Pd^{0} (V)
$\mathbf{C^1}$	−1.25	−0.81
$\mathbf{C^2}$	−1.24	−0.79
$\mathbf{C^3}$	−1.18	−0.82
$\mathbf{C^4}$	−1.10	−0.68

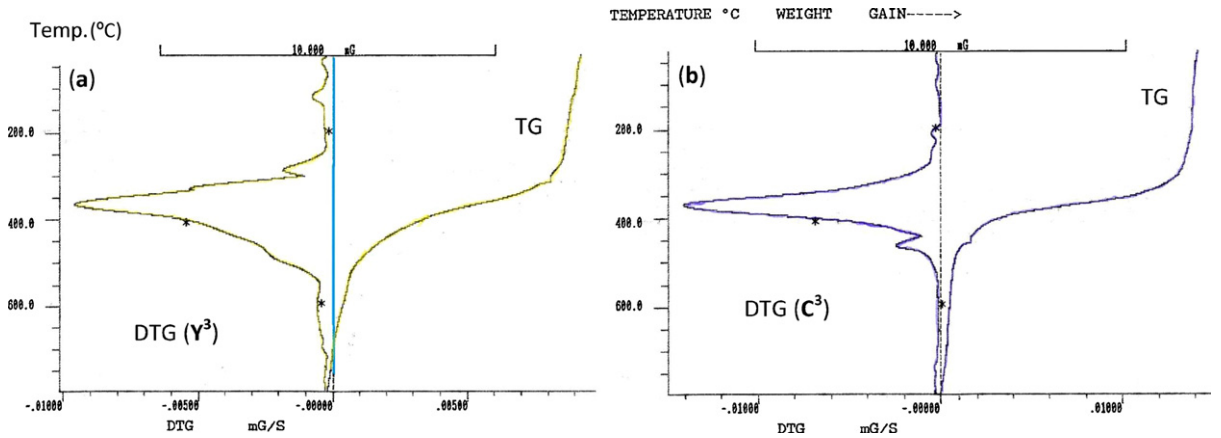

Fig. 4. TG and DTG curves of (a) ylide $\mathbf{Y^3}$ (b) complex $\mathbf{C^3}$.

is accompanied by a mass loss of 80.72% (calcd. 86.72%) may be attributed to the liberation of ylide without bromine atom. The decomposition ended at 797 °C with bromine as a final residue (obs. = 17.49%, calc. = 13.74%). The TG/DTG curves of $\mathbf{C^1}$ (Fig. S8) exhibit three decomposition steps maximized at 391, 615 and 797 °C. The first pronounced peak at 157–593 °C is accompanied by a mass loss amounting to 76.28% (calcd. 75.76%) may be attributed to the liberation of dppe + $\mathbf{Y^1}$ + CF_3. The second decomposition stages at 593–707 °C involve the loss of O_2. The decomposition ended at 797 °C with Pd + SO + SO_3CF_3 as a final residue (obs. = 18.40%, calc. = 21.92%).

For ylide ($\mathbf{Y^3}$), the degradation starts at 25 °C with four decomposition stages centered at 116, 285, 366 and 797 °C (Fig. 4a). The 1st and 2rd decomposition stages are attributed to the degradation of nitro group. The 3rd degradation step is due to the releasing of dppm (obs. = 68.50%, calc. = 70.20%). Decomposition ended at 797 °C with acetophenone as a final residue (obs. = 20.83%, calc. = 21.94%). The TG/DTG curves of complex $\mathbf{C^3}$ (Fig. 4b) exhibited three decomposition steps maximized at 369, 461 and 797 °C. The 1st pronounced peak at 190–439 °C is accompanied by a mass loss amounting to 67.23% (calcd. 66.78%) may be attributed to the liberation of dppe and one ylide ($\mathbf{Y^3}$) without NO_2 group. The second thermal stage, centered at 439–652 °C, is due to the degradation of $3O_2$ with overall mass loss amounting to 21.93% (calcd. 26.40%) leaving two $HSOCF_3$, one NO_2 group and Pd as a final residue.

4.8. X-ray crystallography

Table 3 summarizes crystal and refinement data for $\mathbf{Y^2}$. The molecular structure is shown in Fig. 5. This compound crystallizes in a monoclinic space group $P2_1/c$. As shown, both the phosphine and ylidic components are devoid of steric restrictions and can interact with metal ions and reagents. In the molecule of the title ligand, $\mathbf{Y^2}$, the geometry around the P1 atom is nearly tetrahedral and the O atom is oriented cis to the P atom. The C(27)–C(26)–P(2) [115.3 (3)°] bond angle indicates a distorted trigonal arrangement about C(26). The P(1)-O [2.9104 (16) Å] distance is significantly shorter than the sum of the van der Waals radii of P and O (3.3 A), [86] indicating a strong intermolecular interaction between P^+ and O^-charge centers, which leads to the cis orientation. The P(2)–C(26) [1.711 (5) Å], C(27)–O(1) [1.267 (5) Å] and C(26)–C(27) [1.396 (7) Å] bond lengths within the ylidic fragment are comparable to those observed for the other monoketo ylides [87,88]. Thus, no steric or electronic effects due to the presence of $-CH_2PPh_2$ are anticipated. Also, in this molecule the bond lengths and angles are generally within normal ranges [33]. In ligand $\mathbf{Y^2}$ a combination of several weak and medium

Table 3
Crystal data and structure refinement details for $\mathbf{Y^1}$.

Identification code	$\mathbf{Y^1}$
Empirical formula	$C_{33}H_{28}ClOP_2$
Formula weight	537.94
Temperature (K)	150 (2)
Wavelength (Å)	0.71073
Crystal system space group	Monoclinic $P2_1/c$
Unit cell dimensions (Å)	a = 13.4006 (6) b = 18.6384 (9) c = 11.1601 (5) β = 100.973 (4)°
Volume ($Å^3$)	2736.45
Z, Calculated density (Mg/m^3)	4, 1.306
Absorption coefficient (mm^{-1})	0.282
F (000)	1124.0
Crystal size (mm)	0.65 × 0.30 × 0.13 mm
θ Range for data collection (°)	3.28 to 25.00
Limiting indices	$-15 \le h \le 15$ $-18 \le k \le 22$ $-13 \le l \le 11$
Reflections collected/unique	12500/4794 [R (int) = 0.0687]
Completeness	99.6%
Absorption correction	Semi-empirical from equivalents
Max. and min. transmission	0.964 and 0.838
Refinement method	Full-matrix least-squares on F^2
Data/restraints/parameters	4794/252/395
Goodness-of-fit on F^2	1.119
Final R indices [I > 2 σ (I)]	R_1 = 0.0837, wR_2 = 0.1683
R indices (all data)	R_1 = 0.1361, wR_2 = 0.1871
Largest diff. peak and hole ($eÅ^3$)	1.327 and −0.314

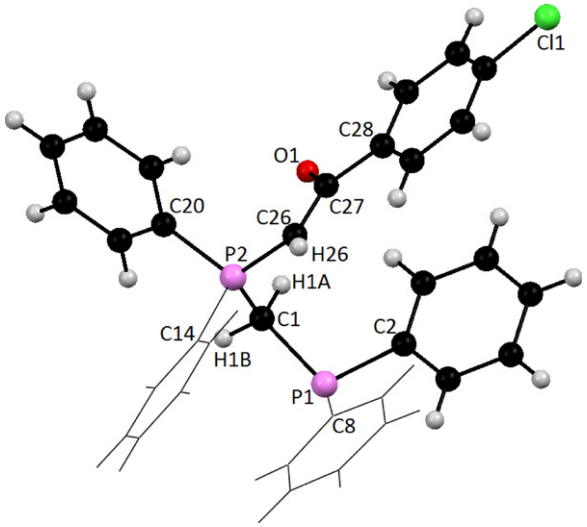

Fig. 5. Molecular structure of $\mathbf{Y^2}$ showing the atom-labeling scheme.

intermolecular interactions, determined the structural assembly in this compound (Fig. 6).

4.9. X-ray powder diffraction

Single crystals of the studied complexes could not be obtained, because the studied complexes are amorphous by nature. The X-ray powder diffraction patterns of the phosphorus ylide ($\mathbf{Y}^3$) and its complex as representative examples were recorded over $2\theta = 5–90^\circ$ in order to obtain an idea about the lattice dynamics of these compounds. A comparison of the obtained XRD patterns of $\mathbf{Y^3}$ and $\mathbf{C}^3$, throws light on the fact that each compound represents a definite compound with a distinct structure (Fig. S9). This identification of the compounds was done by the known method [89]. Such facts suggest that the prepared complexes are amorphous [90]. The X-ray powder diffraction pattern of $\mathbf{Y^3}$ showed a higher degree of crystallinity. The values of 2θ, interplanar spacing d (Å) and the intensities (%) of $\mathbf{Y^3}$ and its complex were tabulated in Table 4. Two peaks characterized to the Pd (II) moiety are also observed at 36.5° and 44.2° [91].

4.10. Theoretical studies

4.10.1. Geometry optimization

The optimized geometries of phosphorus ylide ($\mathbf{Y^2}$) and dppe ligand are depicted in Fig. S10 and the metal complex $\mathbf{C^2}$ is presented in Fig. 7. Representative selected calculated bond parameters for bidentate ligands $\mathbf{Y^2}$ and dppe along with the experimentally determined data are listed in Table 5. The calculated bond lengths and bond angles for both ligands are in good agreement with the corresponding experimental values. As can be seen in Fig. 7, the coordination sphere around the metallic center in complex $\mathbf{C^2}$ is made up of CH_{ylide}, P_{ylide} and two P_{dppe} completing the distorted square planar geometry. The P(3)-Pd-P(4) and C(2)-Pd-P(5) bond angles are 168.3 and 174.6°, respectively,

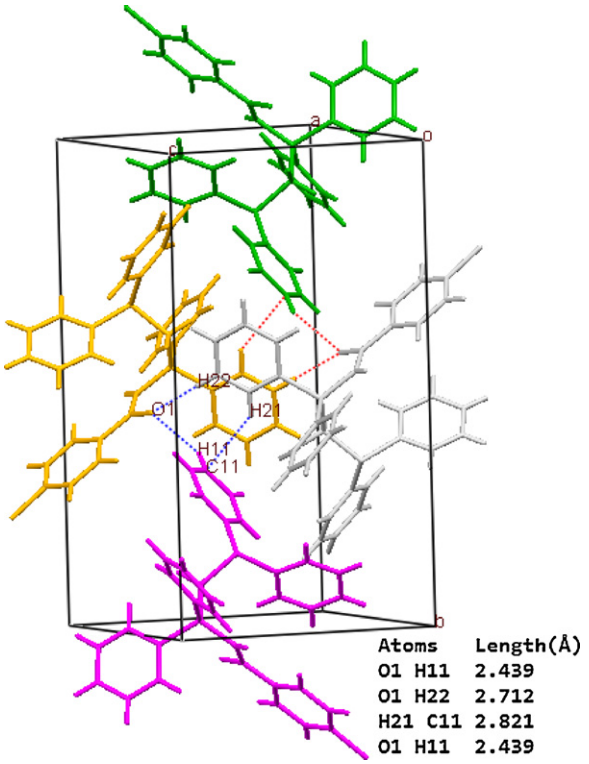

Fig. 6. A representation of ligand $\mathbf{Y^2}$ packing showing the association of the adjacent molecules through C-Hphenyl…πphenyl, C-Hphenyl…Ocarbonyl interactions. Dotted lines represent the short contacts.

indicating that the four donor atoms are not coplanar (Table 6).

4.10.2. ^1H NMR calculations

In order to correctly describe the experimental data, quantum chemical calculations of shielding constants were performed for the optimized structures of $\mathbf{Y^2}$, $\mathbf{C^2}$ and dppe. The absolute isotropic magnetic shielding constants (σ_i) were used to obtain the chemical shifts (Eq. (1)) by referring to the standard compound tetramethylsilane (TMS) for H atoms. The referred compound TMS were calculated at the same levels of theory.

$$\delta_i = \sigma_{TMS} - \sigma_i \quad (1)$$

The shielding constants are presented as chemical shifts and are compared with the corresponding experimental data (Table 7). The computed ^1H chemical shifts of all remarkable protons in these compounds are in good agreement with the corresponding experimental values. As can be seen in Fig. 8, there is a good correlation between the experimental and calculated chemical shifts using both the TZVP and SVP basis sets. Thus it seems that the optimized gas phase structures are close to the structures of these compounds in solution.

4.10.3. ^{31}P NMR calculations

The absolute isotropic chemical shielding values (σ_{iso}) can be converted to chemical shifts (δ) relative to 85%

Table 4
X-ray diffraction data of phosphorus ylide (**Y³**) and Pd complex (**C³**).

Y^3			C^3		
Angle (2θ)	*d*-Value (Å)	Intensity (%)	Angle (2θ)	*d*-Value (Å)	Intensity (%)
3.8	23.22	21.8	2.6	33.95	78.0
6.9	12.80	21.7	3.4	25.96	54.7
8.7	10.15	24.7	3.8	23.23	51.8
9.7	9.11	20.0	7.9	11.18	56.1
12.2	7.24	22.6	8.2	10.77	59.1
12.6	7.01	20.9	9.1	9.71	64.5
13.0	6.80	19.4	9.6	9.20	67.7
13.4	6.60	33.8	10.2	8.66	53.1
13.8	6.41	23.4	10.4	8.49	53.7
14.8	5.98	16.3	11.5	7.68	46.0
16.4	5.40	19.1	15.5	5.71	49.1
16.7	5.30	18.9	15.8	5.60	46.3
17.4	5.09	76.1	16.2	5.46	52.4
18.3	4.84	43.6	16.5	5.36	61.0
19.7	4.50	91.0	17.2	5.15	60.7
20.6	4.30	77.3	17.8	4.97	63.1
22.1	4.01	32.1	18.3	4.84	58.2
22.9	3.88	41.4	18.7	4.74	63.1
23.5	3.78	27.8	19.2	4.61	70.6
24.8	3.58	60.9	19.6	4.52	68.1
25.7	3.46	46.5	20.0	4.43	70.8
26.6	3.34	28.4	20.7	4.28	69.5
28.8	3.09	32.5	21.0	4.22	74.9
30.1	2.96	21.9	21.5	4.12	77.1
30.6	2.91	20.6	22.1	4.01	76.1
31.3	2.85	24.9	22.4	3.96	76.7
31.6	2.82	28.0	22.8	3.89	65.6
32.0	2.79	21.9	23.5	3.78	71.3
33.4	2.68	22.3	23.9	3.72	62.2
41.2	2.18	18.6	24.5	3.63	67.6
			25.5	3.49	64.9
			25.8	3.45	66.0
			28.7	3.10	56.2
			30.4	2.93	60.6
			30.8	2.90	65.4
			31.5	2.83	52.3
			31.8	2.81	53.8
			32.1	2.78	51.8
			33.4	2.68	49.3
			36.5	2.45	45.6
			43.5	2.07	39.4
			44.2	2.04	45.6

aqueous phosphoric acid by comparison to the chemical shielding of PH_3 at the same level of theory [93–96]. Thus we used Eq. (2) which is reported for calculation of phosphorus chemical shifts relative to 85% H_3PO_4 via:

$$\delta(s, calc) = \sigma(PH_3, calc) - \sigma(s, calc) - 266.1 \quad \text{p pm} \qquad (2)$$

Experimental data and theoretical phosphorus electronic shielding calculations of complex **C²**, phosphorus ylide **Y²** and dppe ligand are presented in Table 8.

It should be noted that the precise estimation of phosphorus NMR chemical shift is still an unsolved and very difficult problem [97]. However, the calculated GAIO ^{31}P NMR chemical shifts of four types of phosphorus atom in complex **C²** calculated at bp86/SVP level of theory are very close to the corresponding experimental values.

4.10.4. Interaction energies

The synthesized complexes have $[(dppe)Pd(Y)](OTf)_2$ general formula. We were interested to study the interaction energies of ligands dppe and ylide **Y** with the Pd^{2+} metal ion. Three types of interaction energies in cation of the complex **C²**, $[(dppe)Pd(Y^2)]^{2+}$, were calculated with considering different fragments: (i) Pd^{2+} and both ligands dppe and Y, (ii) $\{(dppe)Pd\}^{2+}$ fragment and Y, (iii) dppe and $\{Pd(Y)\}^{2+}$ fragment. The following equations were used to calculate the interaction energies between the fragments in types i, ii and iii described above.

$$\text{(i)}\ \Delta E_{int} = E_{\left[(dppe)Pd\left(Y^2\right)\right]^{2+}} - \left\{E_{\left[Pd^{2+}\right]} + E_{\left[(dppe)\left(Y^2\right)\right]}\right\}$$

$$\text{(ii)}\ \Delta E_{int} = E_{\left[(dppe)Pd\left(Y^2\right)\right]^{2+}} - \left\{E_{\left[Y^2\right]} + E_{\left[Pd(dppe)\right]^{2+}}\right\}$$

$$\text{(iii)}\ \Delta E_{int} = E_{\left[(dppe)Pd\left(Y^2\right)\right]^{2+}} - \left\{E_{[dppe]} + E_{\left[Pd\left(Y^2\right)\right]^{2+}}\right\}$$

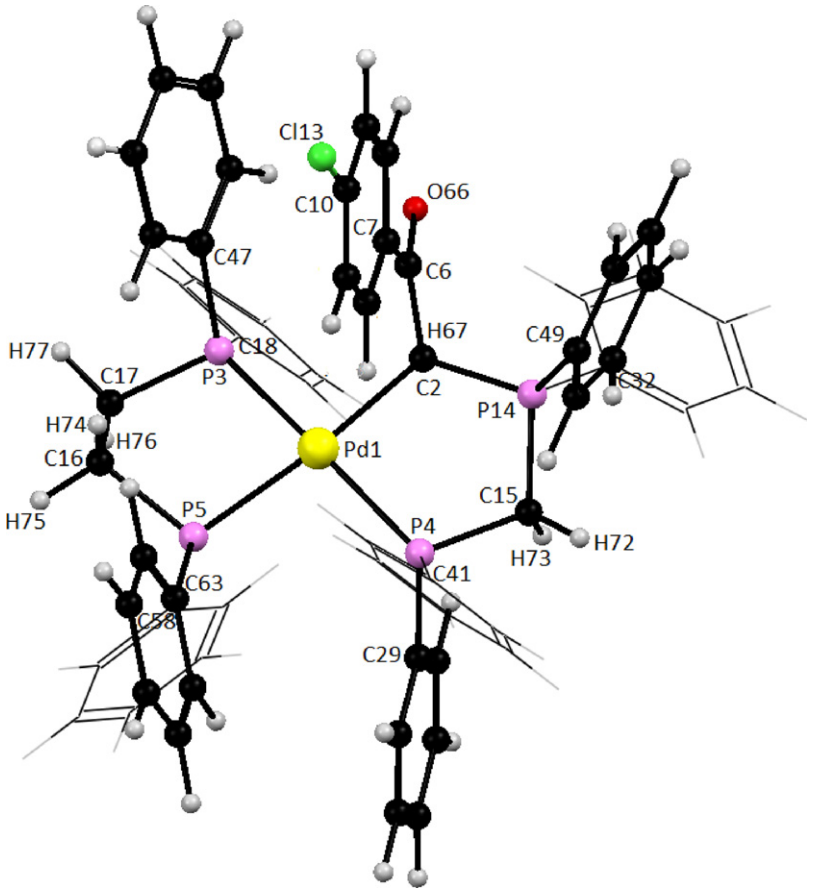

Fig. 7. Optimized structure of complex cation in compound **C²** at Bp86/TZVP level of theory.

Table 5
Selected bond distances (Å) and angles (°) for phosphorus ylide **Y²** and dppe.

	Y²				dppe		
	Exp.	BP86/SVP	BP86/TZVP		Exp. [92]	BP86/SVP	BP86/TZVP
Bond distances				Bond distances			
P2-C11	1.853 (4)	1.907	1.896	P1-C2	1.828 (4)	1.893	1.881
P2-C17	1.81 (2)	1.860	1.847	P1-C7	1.820 (3)	1.862	1.850
P2-C29	1.827 (4)	1.874	1.860	P1-C8	1.818 (4)	1.854	1.842
P10-C11	1.821 (4)	1.852	1.842	C2-C3	1.516 (4)	1.530	1.528
P10-C20	1.799 (5)	1.847	1.832	C2-H29	0.88 (3)	1.112	1.102
P10-C31	1.818 (5)	1.840	1.829	C2-H30	0.96 (3)	1.112	1.102
P10-C1	1.711 (5)	1.742	1.728	C8-C19	1.370 (7)	1.417	1.409
C11-H43	0.989 (4)	1.110	1.101	C8-C23	1.362 (6)	1.415	1.407
C11-H44	0.991 (4)	1.110	1.100	C19-C20	1.375 (10)	1.404	1.396
C1-C3	1.396 (7)	1.418	1.413	C20-C21	1.328 (11)	1.407	1.399
C1-H38	0.89 (4)	1.098	1.088	C21-C22	1.346 (10)	1.405	1.397
C3-O36	1.267 (5)	1.270	1.266	C22-C23	1.382 (8)	1.406	1.399
C3-C4	1.505 (6)	1.513	1.509				
C4-C9	1.385 (6)	1.412	1.404	Bond angles			
C8-C9	1.385 (7)	1.401	1.394	C2-P1-C8	102.6 (3)	103.479	103.691
C7-C8	1.369 (8)	1.407	1.397	C2-P1-C7	100.1 (3)	101.545	101.864
C6-C7	1.378 (7)	1.407	1.397	C7-P1-C8	101.3 (3)	103.283	103.518
C5-C6	1.379 (8)	1.403	1.396	P1-C7-C28	119.0 (5)	125.123	125.217
C4-C5	1.394 (8)	1.413	1.405	P1-C7-C24	123.2 (5)	116.351	116.358
C7-Cl37	1.749 (5)	1.755	1.751	P1-C8-C23	116.7 (6)	121.940	121.877
				P1-C8-C19	125.6 (6)	119.423	119.522
Bond angles				P1-C2-C3	111.1 (4)	118.898	118.829
C17-P2-C29	102.6 (8)	101.466	101.758				
C11-P2-C29	98.8 (2)	97.683	97.896				

Table 5 (*Continued*)

	Y^2			dppe		
	Exp.	BP86/SVP	BP86/TZVP	Exp. [92]	BP86/SVP	BP86/TZVP
P2-C11-P10	107.8 (8)	116.659	117.127			
C11-P10-C31	107.2 (2)	106.537	106.503			
C11-P10-C20	106.7 (2)	105.185	105.532			
C1-P10-C11	113.3 (2)	116.705	116.610			
C1-P10-C31	113.3 (2)	104.958	105.045			
P10-C1-H38	113 (3)	117.095	116.835			
C3-C1-P10	115.3 (3)	116.926	117.816			
C1-C3-O36	121.0 (4)	121.327	121.402			
C4-C3-O36	117.9 (4)	118.453	118.528			
C4-C9-H42	119.2 (5)	117.402	117.777			
C4-C5-H39	120.0 (5)	120.260	120.230			
C8-C7-Cl37	120.0 (4)	119.650	119.575			
C6-C7-Cl37	118.7 (4)	119.525	119.442			

In all cases, the charge of 2+ and a spin multiplicity of 1 were considered for the cation complex and also the fragments containing Pd ion. The calculated electronic energies of all species are given in the supplementary information (Table S1) and calculated interaction energies between the considered fragments are presented in Table 9.

As can be seen, the interaction energy between the $\mathbf{Y^2}$ and $[Pd(dppe)]^{2+}$ fragment in the cation of complex $\mathbf{C^2}$ is more than that between dppe and $[(Y^2)(dppe)]^{2+}$. Furthermore, the sum of the above interaction energies is significantly less than that between the Pd^{2+} ion and $\{(dppe)(Y^2)\}$ fragment which includes both the dppe and $\mathbf{Y^2}$. Thus in order to understand the origin of this considerable difference, we calculated the interaction energy between the Pd^{2+} and each of the dppe and $\mathbf{Y^2}$ alone. As can be seen in Table 9, the interaction energy of the Pd^{2+} ion and $\mathbf{Y^2}$ is larger than that with the dppe, and both are significantly larger than those between the dppe and $[(Y^2)(dppe)]^{2+}$ and/or $\mathbf{Y^2}$ and $[Pd(dppe)]^{2+}$ fragments. Thus the above data reveal three facts; (a) the bonding interaction of a Pd^{2+} ion with a single $\mathbf{Y^2}$ and/or dppe is very large; (b) the bonding interaction of Pd^{2+} ion with the $\mathbf{Y^2}$ is stronger than that between the

Table 6
Selected bond distances (Å) and angles (°) for complex $\mathbf{C^2}$.

Bond distances	BP86/SVP	BP86/TZVP	Bond angles	BP86/SVP	BP86/TZVP
Pd10-C2	2.178	2.197	C2-Pd1-P4	89.297	88.475
Pd1-P3	2.422	2.422	C2-Pd1-P3	90.334	91.296
Pd1-P4	2.373	2.363	C2-Pd1-P5	174.249	174.600
Pd1-P5	2.401	2.379	P3-Pd1-P5	83.960	83.611
P3-C17	1.885	1.870	P3-Pd1-P4	170.315	168.322
P3-C18	1.838	1.828	P4-Pd1-P5	96.449	96.876
P3-C47	1.841	1.830	Pd1-C2-C6	117.579	117.451
P5-C16	1.869	1.856	Pd1-C2-P14	117.536	117.694
P5-C58	1.839	1.827	Pd1-C2-H67	101.196	100.224
P5-C63	1.840	1.829	Pd1-P4-C15	106.967	107.406
P4-C15	1.884	1.871	Pd1-P4-C29	117.606	116.306
P4-C29	1.846	1.835	Pd1-P4-C41	119.085	119.959
P4-C41	1.839	1.828	Pd1-P3-C17	106.802	106.681
C2-C6	1.536	1.532	Pd1-P3-C18	113.699	112.977
C2-P14	1.840	1.822	Pd1-P3-C47	120.802	121.965
C2-H67	1.111	1.103	Pd1-P5-C16	105.434	105.449
P14-C15	1.838	1.828	Pd1-P5-C58	114.958	116.228
P14-C32	1.827	1.816	Pd1-P5-C63	121.344	120.729
P14-C49	1.822	1.808	P3-C17-C16	112.174	111.668
C2-P14	1.840	1.822	P5-C16-C17	109.265	108.765
C15-H72	1.109	1.099	C2-P14-C15	106.897	106.368
C15-H73	1.109	1.100	P4-C15-P14	112.278	112.623
C6-O66	1.237	1.234	C2-C6-O66	117.898	117.760
C6-C7	1.490	1.486	C2-C6-C7	121.260	121.516
C16-C17	1.526	1.524	C7-C6-O66	120.841	120.723
C17-H76	1.110	1.100	P14-C15-H72	111.966	112.210
C17-H77	1.109	1.099	P14-C15-H73	106.056	105.762
C16-H74	1.109	1.099	P3-C17-H76	105.834	106.259
C16-H75	1.111	1.101	P3-C17-H77	108.388	108.684
C10-Cl13	1.737	1.732			

Table 7
The experimental and theoretical ^{1}H NMR chemical shifts (δ, ppm) from TMS for the studied compounds.

Compound	Exp	Calcd[a]		Atom	Assignment
		BP86/SVP	BP86/TZVP		
Dppe	2.1	1.7	1.7	H29	CH_2
	2.1	1.7	1.7	H31	
	2.1	1.8	1.8	H30	
	2.1	1.8	1.8	H32	
Y²	3.6	3.0	3.1	H43	CH_2
	3.6	3.0	3.1	H44	
	4.2	3.8	4.2	H38	CH
	6.9	6.6	6.8	H40	Phenyl-Cl
	6.9	6.8	7.1	H41	
	7.1	6.9	7.1	H39	
	7.1	6.9	8.1	H42	
C²	2.66	1.9	1.5	H76	CH_2
	2.85	2.7	2.3	H75	
	2.66	1.9	1.5	H77	
	2.85	2.7	2.3	H74	
	4.6	3.9	3.7	H73	CH_2
	4.6	3.9	3.7	H72	
	4.8	5.0	4.9	H67	CH
	6.96	6.3	6.2	H69	Phenyl-Cl
	6.98	6.6	6.4	H70	
	6.99	6.8	6.6	H71	
	7.01	7.2	6.9	H68	

[a] Using GIAO method.

Table 8
The experimental and theoretical ^{31}P NMR chemical shifts δ (ppm) from H_3PO_4 for complex **C²**, phosphorus ylide **Y²** and dppe ligand.

Compound	Exp	Calcd[a]		Atoms	Assignment
		BP86/SVP	BP86/TZVP		
dppe	−15	−16.2	96.26	P1	
	−15	−16.2	96.26	P4	
Y²	11	−14.9	99.32	P10	
	−30	−31.5	69.89	P2	
C²	37.4	15.0	11.32	P14	P_d
	19.5	24.0	17.32	P4	P_c
	55.1	48.0	41.37	P5	P_a
	54.9	55.0	48.25	P3	P_b

[a] Using GIAO method.

Pd^{2+} and dppe; (c) the first coordinated bidentate ligand decreases significantly the interaction energy of the metal ion (the resulting fragment) with the second bidentate ligand.

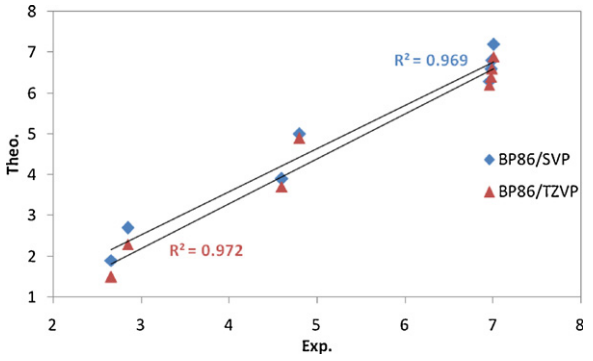

Fig. 8. Correlation between theoretical and corresponding experimental values (δ, ppm) of ^{1}H chemical shifts for complex **C²**.

4.11. Biological activity

4.11.1. DPPH radical scavenging assay

DPPH assay provided information on the reactivity of the complexes with a stable free radical. Because of the odd electron, DPPH shows a strong absorption band at 517 nm in visible spectrophotometery. As this electron becomes paired off in the presence of free radical scavenger, the absorption vanishes and the resulting decolorization is stoichiometric with respect to the number of electrons taken up [48]. Antioxidant properties, especially radical scavenging activities, are very important due to the deleterious role of free radicals in foods and biological systems [98]. Assessment of antioxidant activities showed that activity of the complexes in scavenging of free radical DPPH is fairly good but less than ascorbic acid (79.61%) as positive control. However there are no significant differences between scavenging ability of the free radical DPPH of complexes (Table 10). Antioxidant activities of the complexes did not promoted by increasing concentration.

Table 9
Interaction energies in $[(dppe)Pd(Y^2)]^{2+}$ cation of complex **C²** with considering different fragments.

Method	ΔE_{int}				
	Pd^{2+}: $[(Y^2)(dppe)]$	$[Pd(dppe)]^{2+}$: (Y^2)	$[Pd(Y^2)]^{2+}$: (dppe)	Pd^{2+}: (Y)	Pd^{2+}: (dppe)
BP86/SVP	−1070.531	−139.307	−122.364	−980.797	−946.284
BP86/TZVP	−1039.155	−131.149	−119.854	−949.421	−922.438

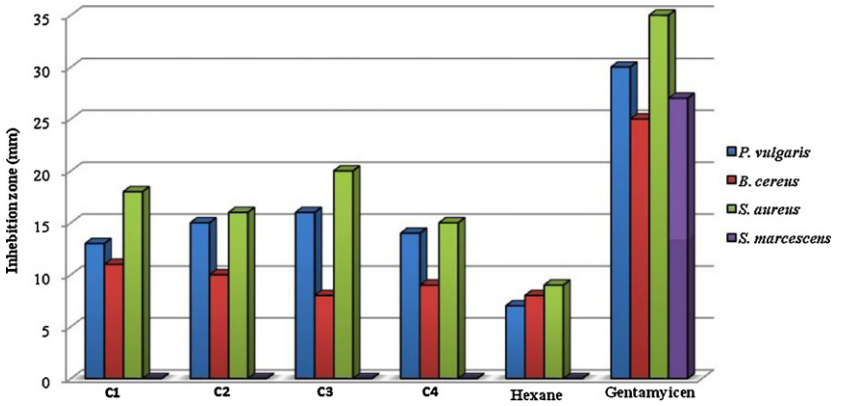

Fig. 9. Antibacterial activities of the studied samples (at 1 mg/ml concentration), negative control (Hexane), and positive control (GM).

4.11.2. Antibacterial activity

All complexes showed antibacterial activities against bacteria tested especially on Gram positive ones. In contrast, *Serratia marcescens* (-) was the most resistant bacterium (Table 11). When antimicrobial activities of the tested samples were compared with those of reference antibiotics, the inhibitory potency of the tested complexes was found to be remarkable (Fig. 9). Although all bacteria tested are resistant to Penicillin, the antibacterial effects of all complexes were higher than those of Penicillin on these bacteria. As it is well known, *S. aureus* and *Bacillus* species, especially *B. cereus*, are agents of food poisoning [99].

However, today it is known that the synergistic or antagonistic effect of one compound in minor percentage of mixture has to be considered. These complexes showed more activity against some bacteria under indicial experimental conditions. This would suggest that the structure of complexes may reduce the polarity of the metal ion mainly. Also, we can consider that the coordination may facilitate the ability of a complex to cross the lipid layer of the bacterial cell membrane and in this way may be affect the mechanisms of growth and development of microorganisms [100,101]. As can be seen in Table 11, the presence of Br, Cl, NO2 and OCH3 groups exerts a number of changes on antibacterial activities of the tested complexes. So, in case of **C³**, the presence of NO_2 moiety induced an increase of their action against most of bacteria, while complex **C⁴** was found to have low activity against bacteria. The above results indicate that the complexes studied may be used in treatment of diseases caused by bacteria tested. However, further studies are needed to evaluate the in vivo potential of these compounds in animal models.

Table 10
Comparison of DPPH radical scavenging abilities of the studied complexes and ascorbic acid.

Compounds	Concentration mg/ml (μM/l)	DPPH scavenging (%)
C¹	0.2 (92.75)	28.10 ± 2.8^a
	0.4 (123.6)	28.16 ± 2.6^a
	0.6 (185.5)	29.55 ± 3.2^a
	0.8 (371.0)	31.14 ± 1.8^{ab}
	1 (742.0)	35.80 ± 2.5^b
	Average	30.55^a
C²	0.2 (93.25)	30.11 ± 2.5^a
	0.4 (124.3)	31.85 ± 3.4^a
	0.6 (186.5)	32.50 ± 1.8^a
	0.8 (373.0)	32.38 ± 2.0^a
	1 (746.0)	37.46 ± 2.7^b
	Average	32.86^a
C³	0.2 (92.5)	34.08 ± 2.0^a
	0.4 (123.3)	34.45 ± 2.4^a
	0.6 (185.0)	35.10 ± 1.4^a
	0.8 (370.0)	35.80 ± 1.9^a
	1 (740.0)	38.20 ± 2.6^a
	Average	35.53^a
C⁴	0.2 (93.6)	29.95 ± 2.9^a
	0.4 (124.8)	30.15 ± 1.7^a
	0.6 (187.25)	30.25 ± 2.5^a
	0.8 (374.0)	33.20 ± 1.5^a
	1 (749.0)	34.80 ± 2.1^a
	Average	31.67^a
Ascorbic acid	0.2 (709.75)	75.00 ± 0.8^a
	0.4 (946.3)	80.84 ± 1.5^a
	0.6 (1419.5)	81.21 ± 1.4^b
	0.8 (2839.0)	$80.84b \pm 2.2^b$
	1 (5678.0)	$80.16b \pm 1.9^b$
	Average	79.61^b

Experiment was performed in triplicate and expressed as mean ± SD. Values along each column with different superscripts are significantly different ($P < 0.05$)

Table 11
Antibacterial activities of the studied complexes at different concentrations mg/ml (μM/l).

Microorganism	Inhibition zone diameter (mm)													
	C¹			**C²**			**C³**			**C⁴**			Solution	Antibiotic
	1 (742)	0.1 (74.2)	0.01 (7.42)	1 (746)	0.1 (74.6)	0.01 (7.46)	1 (740)	0.1 (74.0)	0.01 (7.40)	1 (749)	0.1 (74.9)	0.01 (7.49)	Hexane	Gentamycin
P. vulgaris (−)	13[a]	11[b]	9c	15[a]	11[b]	8[c]	16[a]	14[b]	10[c]	14[a]	12[b]	8[c]	7	30
B. cereus (+)	11[a]	na	na	10[a]	8[b]	na	8[a]	na	na	9a	8b	na	8	25
S. aureus (+)	18[a]	11[b]	na	16[a]	12[b]	10[c]	20[a]	15[b]	11[c]	15[a]	11[b]	10c	9	35
S. marcescens (−)	na	na	na	na	na	na	na	na	na	na	na	na	na	27

Values along column with different superscript are significantly different ($P < 0.05$). na: no active.

5. Conclusion

The present study describes the very simple and efficient synthesis and characterization of a series of chelate Pd (II) complexes. The coordination ability of the phosphorus ylides and dppe has been proved in the complexation reaction with Pd (II) ion. Based on the results obtained from the physicochemical techniques of the metal complexes, one can conclude that the studied ligands behaves as a neutral bidentate ligand coordinated to the metal ion via phosphorus atoms of dppe in one side, and via terminal phosphorus atom (Pc) and methene group (CH) of the ylide on the other side. Thus, distorted square planar geometry is suggested for the studied complexes. In these distorted square planar complexes the three P-substituted atoms are coordinated; the fourth coordination site is filled with a methene group. Theoretical studies confirm a distorted square planner structure for the complex cation in **C²** and probably other complexes. There is an excellent correlation between the calculated and experimental ^{1}H NMR chemical shifts for latter complex. Calculated data also show that the bonding interaction of Pd^{2+} ion with the **Y²** is stronger than that between the Pd^{2+} and dppe. Results from present study clearly demonstrated that the complexes exhibit antioxidant and antibacterial properties that might be helpful in preventing the progress of various diseases and can be used in an alternative system of medicine. However, possible side deleterious effects of these complexes on human health should be more investigated.

Acknowledgment

This work was supported by Bu-Ali Sina University funds. We thank Mrs. Akhlaghi for recording ESI-MS spectra. Our gratitude also goes to Mr. Zebarjadian for recording NMR spectra.

Appendix A. Supplementary data

Supplementary data associated with this article can be found, in the online version, at http://dx.doi.org/10.1016/j.crci.2012.10.006.

CCDC 753848 contains the supplementary crystallographic data for the ligand Y2. These data can be obtained free of charge via www.ccdc.cam.ac.uk/data_request/cif or from the Cambridge Crystallographic Data Center, 12, Union Road, Cambridge CB2 1EZ, UK. Tel.: +44 0 1223 762911; or deposit@ccdc.cam.ac.uk.

References

[1] M. Juribašić, K. Molčanov, B. Kojić-Prodić, L. Bellotto, M. Kralj, F. Zani, L. Tušek-Božić, J. Inorg. Biochem. 105 (2011) 867.
[2] H. Khan, A. Badshah, G. Murtaz, M. Said, Z. Rehman, C. Neuhausen, M. Todorova, B.J. Jean-Claude, I.S. Butler, Eur. J. Med. Chem. 46 (2011) 4071.
[3] A.K. Mishra, N.K. Kaushik, Eur. J. Med. Chem. 42 (2007) 1239.
[4] N.T.A. Ghani, A.M. Mansour, Eur. J. Med. Chem. 47 (2012) 399.
[5] T. Rosu, E. Pahontu, S. Pasculescu, R. Georgescu, N. Stanica, A. Curaj, A. Popescu, M. Leabu, Eur. J. Med. Chem. 45 (2010) 1627.
[6] S.A. Khan, M. Yusuf, Eur. J. Med. Chem. 44 (2009) 2270.
[7] N.T.A. Ghani, A.M. Mansour, Inorg. Chim. Acta 373 (2011) 249.
[8] A.S. Abu-Surrah, H.H. Al-Saõdoni, M.Y. Abdalla, Cancer Ther. 6 (2008) 1.
[9] H.O.U. Wen-Chi, W.U. Wen-Chung, Y.A.N.G. Chih-Yuan, C.H.E.N. Hsien-Jung, L.I.U. Sin-Yie, L.I.N. Yaw-Huei, Bot. Bull. Acad. Sin. 45 (2000) 285.
[10] J.M.C. Gutteridge, Chem. Biol. Interact. 91 (1994) 133.
[11] K.A. Steinmetz, J.D. Potter, J. Am. Diet. Assoc. 96 (1996) 1027.
[12] O.I. Aruoma, J. Am. Oil. Chem. Soc. 75 (1998) 199.
[13] A. Pieroni, V. Janiak, C.M. Dürr, S. Lüdeke, E. Trachsel, M. Heincrich, Phytother. Res. 16 (2002) 467.
[14] B. Li, S. Yu, J.Y. Hwang, S. Shi, J. Miner, Mater. Charact. Eng. 1 (2002) 61.
[15] P.M. Bennett, Br. J. Pharmacol. 153 (2008) 347.
[16] G.D. Wright, Chem. Biol. 7 (2000) 127.
[17] S. Gibbons, Phytochem. Rev. 4 (2005) 63.
[18] W.C. Kaska, Coord. Chem. Rev. 48 (1983) 1.
[19] U. Belluco, R.A. Michelin, M. Mozzon, R. Bertani, G. Facchin, L. Zanotto, L. Pandolfo, J. Organomet. Chem. 557 (1998) 37.
[20] L.R. Falvello, S. Fernandez, R. Navarro, A. Rueda, E.P. Urriolabeitia, Inorg. Chem. 37 (1998) 6007.
[21] R. Navarro, E.P. Urriolabeitia, J. Chem. Soc. Dalton Trans. (1999) 4111.
[22] H. Schmidbaur, Angew. Chem. 22 (1983) 907.
[23] L.R. Falvello, S. Fernandez, R. Navarro, A. Rueda, E.P. Urriolabeitia, Organometallics 17 (1998) 5887.
[24] Y. Oosawa, H. Urabe, T. Saito, Y. Sasaki, J. Organomet. Chem. 122 (1976) 113.
[25] S.J. Sabounchei, S. Samiee, D. Nematollahi, A. Naghipour, D. Morales-Morales, Inorg. Chim. Acta 363 (2010) 3973.
[26] A. Spannenberg, W. Baumann, U. Rosenthal, Organometallics 19 (2000) 3991.
[27] D. Saravanabharathi, T.S. Venkatakrishnan, M. Nethaji, S.S. Krishnamurthy, Proc. Ind. Acad. Sci. (Chem. Sci.) 115 (2003) 741.
[28] I.J.B. Lin, H.C. Shy, C.W. Liu, L.K. Liu, S.K. Yeh, J. Chem. Soc. Dalton Trans. 8 (1990) 2509.
[29] L.R. Falvello, S. Fernandez, R. Navarro, E.P. Urriolabeitia, Inorg. Chem. 39 (2000) 2957.
[30] H. Takahashi, Y. Oosawa, A. Kobayashi, T. Saito, Y. Sasaki, Chem. Lett. (1976) 15.
[31] H. Takahashi, Y. Oosawa, A. Kobayashi, T. Saito, Y. Sasaki, Bull. Chem. Soc. Jpn. 50 (1977) 1771.
[32] R. Uson, J. Fornies, R. Navarro, A.M. Ortega, J. Organomet. Chem. 334 (1987) 389.
[33] M.M. Ebrahima, K. Panchanatheswaran, A. Neels, H. Stoeckli-Evans, J. Organomet. Chem. 694 (2009) 643.
[34] S.M. Sbovata, A. Tassan, G. Facchin, Inorg. Chim. Acta 361 (2008) 3177.
[35] M.M. Ebrahim, H. Stoeckli-Evans, K. Panchanatheswaran, Polyhedron 26 (2007) 3491.

[36] A.S. Batsanov, J.A.K. Howard, G.S. Robertson, M. Kilner, Acta Crystallogr. Sect. E 57 (2001) 301.
[37] A.X.S. Bruker, SAINT Software Reference Manual, 5465 E, Cheryl Parkway, Madison, WI 53711-5373, USA, 1998.
[38] G.M. Sheldrick, Acta Crystallogr. Sect. A 46 (1990) 467.
[39] G.M. Sheldrick, SHELXL-97, Program for Crystal Structure Refinement, University of Göttingen, Germany, 1998.
[40] L.J. Farrugia, J. Appl. Crystallogr. 30 (1997) 565.
[41] F. Weigend, R. Ahlrichs, Phys. Chem. Chem. Phys. 7 (2005) 3297.
[42] A.D. Becke, Phys. Rev. A 38 (1988) 3098.
[43] J.P. Perdew, Phys. Rev. B 33 (1986) 8822.
[44] M.J. Frisch, et al. Gaussian 03, revision D.01, Gaussian, Inc., Wallingford, CT, 2004.
[45] K. Wolinski, J.F. Hinton, P. Pulay, J. Am. Chem. Soc. 112 (1990) 8251.
[46] G. Magyarfalvi, P. Pulay, J. Chem. Phys. 119 (2003) 1350.
[47] L.L. Mensor, F.S. Menezes, G.G. Leitao, A.S. Reis, T.S. Santos, C.S. Coube, Phytother. Res. 15 (2001) 127.
[48] A.W. Bauer, M.M. Kirby, J.C. Sherris, M. Truck, Am. J. Clin. Pathol. 45 (1966) 493.
[49] G. Annibale, P. Bergamini, V. Bertolasi, M. Cattabriga, V. Ferretti, Inorg. Chem. Commun. 3 (2000) 303.
[50] M. Agostinho, P. Braunstein, C. R. Chimie 10 (2007) 666.
[51] M. Fuss, H.U. Siehl, Organometallics 18 (1999) 758.
[52] S.J. Sabounchei, S. Samiee, S. Salehzadeha, Z.B. Nojini, E. Irran, J. Organomet. Chem. 695 (2010) 1441.
[53] S.J. Sabounchei, S. Samiee, S. Salehzadeha, M. Bayat, Z.B. Nojini, D. Morales-Morales, Inorg. Chim. Acta 363 (2010) 1254.
[54] M. Kalyanasundari, K. Panchanatheswaran, W.T. Robinson, H. Wen, J. Organomet. Chem. 491 (1995) 103.
[55] P. Braunstein, Y. Chauvin, J. Nahring, A. DeCian, J. Fischer, A. Tiripicchio, F. Ugozzoli, Organometallics 15 (1996) 5551.
[56] L. Dahlenburg, K. Herbst, M. Kuhnlein, Z. Anorg. Allg. Chem. 623 (1997) 250.
[57] M. Lamac, I. Cisarova, P. Stepnicka, J. Organomet. Chem. 690 (2005) 4285.
[58] A.M. Trzeciak, J.J. Ziolkowski, T. Lis, R. Choukroun, J. Organomet. Chem. 575 (1999) 87.
[59] P. Stepnicka, I. Cisarova, J. Chem. Soc. Dalton Trans. (1998) 2807.
[60] A.M. Trzeciak, P. Stepnicka, E. Mieczynska, J.J. Ziolkowski, J. Organomet. Chem. 690 (2005) 3260.
[61] P.S. Pregosin, R.W. Kunz, IR and NMR of transition metal phosphine complexes, Springer-Verlag, West Berlin, 1979.
[62] I.J. Colquhoun, W. McFarlane, J. Chem. Soc. Dalton Trans. 17 (1977) 1674.
[63] A. Bright, B.E. Mann, C. Masters, B.L. Shaw, R.M. Slade, R.E. Stainbank, J. Chem. Soc. A 0 (1971) 1826.
[64] P. Braunstein, Y. Chauvin, J. Fischer, H. Olivier, C. Strohmann, D.V. Toronto, New J. Chem. 24 (2000) 437.
[65] R. Prabhakaran, S.V. Renukadevi, R. Karvembu, R. Huang, J. Mautz, G. Huttner, R. Subashkumar, K. Natarajan, Eur. J. Med. Chem. 43 (2008) 268.
[66] J.A. Teagle, J.L. Burmeister, Inorg. Chim. Acta 118 (1986) 65.
[67] S.J. Sabounchei, M. Ahmadi Gharacheh, H.R. Khavasi, J. Coord. Chem. 63 (2010) 1165.
[68] A.P. Rebolledo, M. Vieites, D. Gambino, O.E. Piro, E.E. Castellano, C.L. Zani, E.M. Souza-Fagundes, L.R. Teixeira, A.A. Batista, H. Beraldo, J. Inorg. Biochem. 99 (2005) 698.
[69] D. Kovala-Demertzi, A. Domopoulou, M.A. Demervzis, G. Valle, A. Papageorgiou, J. Inorg. Biochem. 68 (1997) 147.
[70] P.I. da, S. Maia, A.G. de, A. Fernandes, J.J.N. Silva, A.D. Andricopulo, S.S. Lemos, E.S. Lang, U. Abram, V.M. Deflon, J. Inorg. Biochem. 104 (2010) 1276.
[71] L. Papathanasis, M.A. Demertzis, P.N. Yadav, D. Kovala-Demertzi, C. Prentjas, A. Castiñeiras, S. Skoulika, D.X. West, Inorg. Chim. Acta 357 (2004) 4113.
[72] E. Kwiatkowski, M. Kwiatkowski, Inorg. Chim. Acta 90 (1984) 145.
[73] E. Kwiatkowski, M. Kwiatkowski, Inorg. Chim. Acta 117 (1986) 145.
[74] Y.P. Tiam, C.Y. Duan, Z.L. Lu, X.Z. You, Polyhedron 15 (1996) 2263.
[75] S. Dey, V.K. Jain, A. Knoedler, W. Kaim, Indian J. Chem. 42A (2003) 2339.
[76] D.M. Boghaei, S. Mohebi, J. Chem. Res. 6 (2001) 224.
[77] S.O. Ajay, D.R. Goddard, J. Chem. Soc. A 0 (1971) 2673.
[78] M.J.M. Campbell, A.J. Collis, R. Grzeskowiak, J. Inorg. Nucl. Chem. 38 (1976) 173.
[79] A.B.P. Lever, Inorganic electronic spectroscopy, second ed, Elsevier, Amsterdam, 1982pp. 544.
[80] D.X. West, M.S. Lockwood, A. Liberta, X. Chen, R.D. Willet, Trans. Met. Chem. 18 (1993) 221.
[81] S.P. Perlepes, P. Jacobs, H.O. Desseyn, J.M. Tasangaris, Spectrochim. Acta A 43 (1987) 771.
[82] R.J. Batchelor, F.W.B. Einstein, I.D. Gay, J. Gu, B.M. Pinto, X. Zhou, Inorg. Chem. 35 (1996) 3667.
[83] N.R. Champness, P.F. Kelly, W. Levason, G. Reid, A.M.Z. Slawin, D. Williams, Inorg. Chem. 34 (1995) 651.
[84] A.J. Downard, A.M. Bond, A.J. Clayton, L.R. Hanton, D.A. McMorran, Inorg. Chem. 35 (1996) 7684.
[85] A. Álvarez-Lueje, C. Zapata-Urzúa, S. Brain-Isasi, M. Pérez-Ortiz, L. Barros, H. Pessoa-Mahana, M.J. Kogan, Talanta 79 (2009) 687.
[86] J.D. Dunitz, X-ray analysis and the structure of organic molecules, Cornell University Press, Ithaca, 1979.
[87] S.J. Sabounchei, H. Nemattalab, H.R. Khavasi, Anal. Sci. 26 (2009) 35.
[88] S.J. Sabounchei, A. Dadras, M. Jafarzadeh, H.R. Khavasi, Acta Cryst. E63 (2007) 3160.
[89] B.D. Cullity, Elements of X-ray diffraction, Second ed., Addison-Wesley Publishing Company, Inc., Boston, 1978.
[90] N.T.A. Ghani, A.M. Mansour, J. Mol. Struct. 991 (2011) 108.
[91] P. Karthikeyan, P.N. Muskawar, S.A. Aswar, P.R. Bhagat, S.K. Sythana, J. Mol. Cat. A 358 (2012) 112.
[92] A.S. Batsanov, J.A.K. Howard, G.S. Robertson, M. Kilner, Acta Cryst. E57 (2001) 301.
[93] B. Cromp, T. Carrington, D.R. Salahub, J. Chem. Phys. 110 (1999) 7153.
[94] T.M. Alam, Int. J. Mol. Sci. 3 (2002) 888.
[95] C.J. Jameson, A.C. De Dios, A.K. Jameson, Chem. Phys. Lett. 167 (1990) 575.
[96] C.J. Jameson, Annu. Rev. Phys. Chem. 47 (1996) 135.
[97] T. Ruman, K. Długopolska, A. Jurkiewicz, D. Rut, T. Frączyk, J. Cieśla, A. Leś, Z. Szewczuk, W. Rode, Bioorg. Chem. 38 (2010) 74.
[98] C.A. Rice-Evans, N.J. Miller, G. Paganga, Free Radic. Biol. Med. 20 (1996) 933.
[99] S. Burt, Inter. J. Food Microbiol. 94 (2004) 223.
[100] N. Fahmi, I.J. Gupta, R.V. Singh, Phosphorus, Sulfur Silicon Relat. Elem. 132 (1998) 1.
[101] M. Tumer, D. Ekinci, F. Tumer, A. Bulut, Spectrochim. Acta A 67 (2007) 916.